CRYSTAL GROWTH & DESIGN
2009
VOL. 9, NO. 7
3044–3051

Selective Crystallization of the Metastable α-Form of L-Glutamic Acid using Concentration Feedback Control

Nicholas C. S. Kee,[†,‡,§] Reginald B. H. Tan,[‡,§] and Richard D. Braatz*[,†]

Department of Chemical and Biomolecular Engineering, University of Illinois at Urbana-Champaign, 600 South Mathews Avenue, Urbana, Illinois 61801, Department of Chemical and Biomolecular Engineering, National University of Singapore, 4 Engineering Drive 4, Singapore 117576, and Institute of Chemical and Engineering Sciences, 1 Pesek Road, Jurong Island, Singapore 627833

Received May 23, 2008; Revised Manuscript Received March 16, 2009

ABSTRACT: A systematic methodology is presented for the selective crystallization of the metastable form of a monotropic dimorph, L-glutamic acid, for batch cooling crystallization. Attenuated total reflection-Fourier transform infrared (ATR-FTIR) spectroscopy coupled with chemometrics was used to determine the solute concentration and solubility curves of both α- and β-forms of L-glutamic acid in aqueous solution. The metastable limit associated with secondary nucleation for a seeded system was determined using laser backscattering (focused beam reflectance measurement, FBRM). Batch crystallizations seeded with the metastable α-form crystals following various preset supersaturation profiles were implemented using concentration feedback control which regulated the cooling rate based on the in situ measurement of solute concentration. Batch crystallizations operated at constant relative supersaturation in an appropriate temperature range prevented secondary nucleation of both polymorph types and were successful in selectively growing large metastable crystals with uniform size.

Introduction

With the increasing structural complexity of high value-added products, multiple polymorphs[1] (different crystalline arrangements of the same compound) are more frequently encountered in the pharmaceutical industry. Although chemically identical, the different polymorphs display a variation in their physical properties such as crystal morphology, density, solubility, and color. These in turn exert an influence on the performance of the product, for example, the bioavailability and shelf-life of pharmaceutical compounds. It is pertinent to have a consistent and reliable production process for the targeted polymorph for feasible economic yield as well as for compliance of regulatory aspects. It is often possible to obtain the thermodynamically stable form without much complication under suitable crystallization conditions such as temperature and agitation rate, for a long enough batch experiment. Producing crystals of the metastable form in a controlled and repeatable manner is more challenging, the main challenge being to prevent cross nucleation of the stable form. Methods developed for the selective crystallization of the metastable form include identifying a critical level of seed loading necessary to suppress secondary nucleation of both polymorphs[2] and fines dissolution[3] in the case of glycine, as well as using additives to stabilize the metastable form by conformational mimicry for L-glutamic (L-glu) acid.[4] These implementations are system specific with uncertain applicability to other polymorphic systems.

A strategy for selective crystallization based on the solubility diagrams is more generic.[5−8] These strategies are based on seeding locations or spontaneous nucleation of the targeted form in its occurrence domain[9] and more importantly, following a specified trajectory in the phase diagram so that the combined effects of desaturation due to crystal nucleation and growth and supersaturation due to cooling or antisolvent addition do not drive the solute concentration into the domains of spontaneous nucleation of the undesired forms.[7,8] For a monotropic system with two different positions for the metastable limit, the thermodynamically stable polymorph, Form II, could be selectively produced by operating from x to y as shown in Figure 1a. An undersaturated solution is cooled from x, seeded with Form II crystals after crossing its solubility curve, $C_{sat,II}$, and cooled with the supersaturation profile below the metastable limit to y, which avoids uncontrolled nucleation. Alternatively, Form II can also be obtained by following a supersaturation profile below the Form I solubility curve, $C_{sat,I}$, while exceeding the shown metastable limit. As this operation is still between the solubility curves, the resulting nucleation produces only Form II, which widens the product size distribution but does not affect polymorph purity. Seeding and controlled growth of the metastable polymorph, Form I, is not possible for a system as in Figure 1a.[8]

With the metastable limit between the solubility curves, it is difficult to produce crystals with high polymorph purity for Form I in regions supersaturated with respect to this form, due to the high likelihood of nucleating some unwanted Form II once the metastable limit is crossed. The production of highly pure Form I crystals is much more promising for a monotropic system with characteristics as shown in Figure 1b. Form I can be obtained by operating from x to y with seeding of Form I just after crossing its solubility curve.[8] For pharmaceutical systems, the metastable zone tends to be wide, in which case the schematic in Figure 1b is much more likely, providing an opportunity to crystallize the metastable form. Similar operations can be applied to an enantiotropic dimorph system (Figure 2).[7]

The schematics in Figures 1 and 2 show only a single metastable limit instead of one for each form[7] as it is difficult to experimentally determine two distinct metastable limits for some systems.[10] Crossing the metastable limit in regions supersaturated with respect to both forms could potentially nucleate either or even concomitant forms depending on the process conditions such as the solvent type, temperature range, and seed form. Such operations should be avoided if selective growth of a polymorphic form is desired.

* Corresponding author: Phone: 217-333-5073. Fax: 217-333-5052. E-mail: braatz@uiuc.edu.
[†] University of Illinois at Urbana-Champaign.
[‡] National University of Singapore.
[§] Institute of Chemical and Engineering Sciences.

10.1021/cg800546u CCC: $40.75
Published on Web 06/03/2009

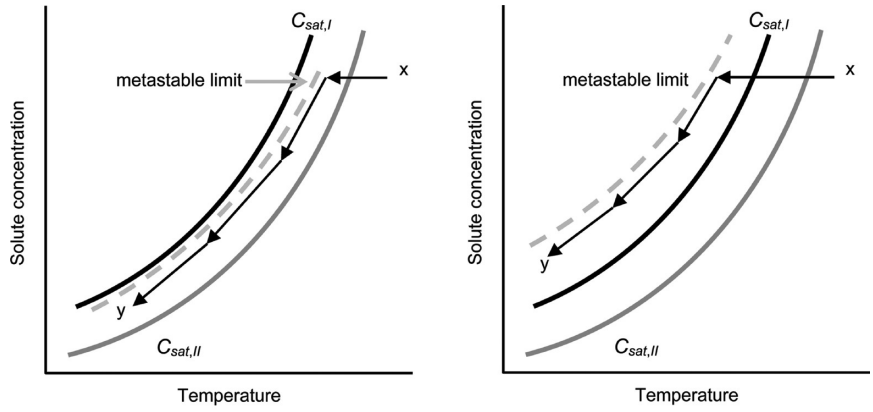

Figure 1. Schematic of selective crystallization operations for (a) Form II and (b) Form I, in a monotropic dimorph system based on the solubility diagram.

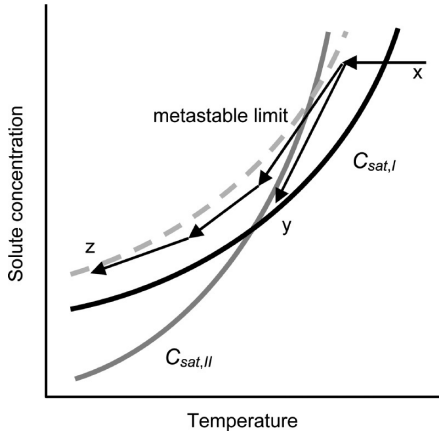

Figure 2. Schematic of selective seeded crystallization operations for Form I, in an enantiotropic dimorph system based on the solubility diagram. The path from *x* to *y* can only produce Form I, whereas the path from *x* to *z* will produce Form I with higher yield provided that nucleation of Form II can be suppressed.

The above techniques rely on early seeding with the targeted form, as opposed to relying on nucleation of that form. Central to the implementation of such operations is the control of the cooling or antisolvent addition rate to balance desaturation due to crystallization and increased supersaturation caused by cooling or other means, so that the supersaturation profile remains within a specified region of the phase diagram. Concentration feedback control has the capability to operate the crystallization to follow the desired concentration profile. Concentration feedback control allows the operation of the crystallizer based on the solute concentration measurement so that it follows a supersaturation profile within the metastable zone to avoid unwanted nucleation, which would otherwise widen the product crystal size distribution.[11−14] The controller compares the solute concentration measured in situ to some concentration set point, and adjusts the cooling or antisolvent addition rate accordingly so that the preset concentration curve is followed.[14,15] This concentration control strategy, which does not require accurate kinetic data or repetitive trials, has shown improved robustness against variation in growth or nucleation kinetics and practical disturbances in batch cooling and antisolvent crystallizations, compared to classical recipes.[5,6,15,16] This paper describes the application of this concentration control methodology for the selective crystallization of a metastable polymorph of L-glu acid in aqueous solution.

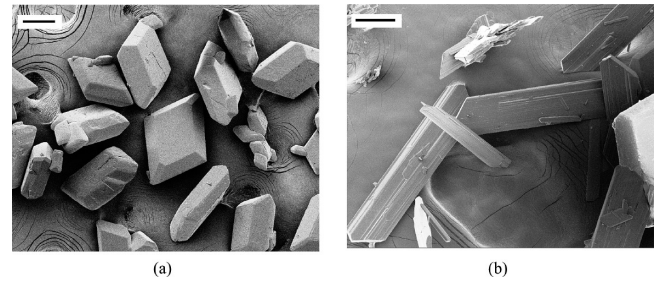

Figure 3. Scanning electron micrographs of L-glu acid crystals (scale bar 100 μm): (a) α-form, (b) β-form.

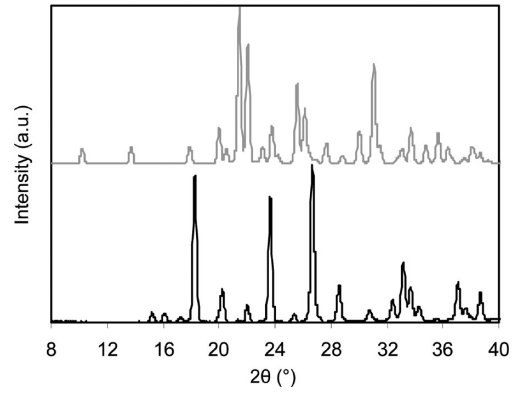

Figure 4. PXRD patterns of α (bottom) and β (top) forms of L-glu acid.

L-Glu acid crystals have two known polymorphs, α- and β-forms, which are monotropically related.[17] The α-form has a prismatic (Figure 3a) or granular morphology if precipitated at low supersaturation,[17] while the β-form crystallizes as needlelike platelets (Figure 3b). In industrial processing, the α-form is preferred as it is easier to handle in subsequent downstream operations.[18] Numerous papers have studied the polymorphic transformation behavior of L-glu acid.[17,19−23] At 45 °C or higher, excess amounts of the α-form in a saturated aqueous solution will transform into the stable β-form. The transformation is solvent-mediated and consists of two steps: the dissolution of the α-form and the nucleation and growth of the β-form, which is the rate-determining step.[17] The transformation has a strong

Table 1. ATR-FTIR Calibration Samples for Solute Concentration Measurement

calibration sample	solute concentration (g/g solvent)	temperature range (°C)	number of spectra
Cs1	0.00837	33.7−21.0	21
Cs2	0.01301	48.0−23.3	40
Cs3	0.01800	56.7−32.3	40
Cs4	0.02300	64.0−34.1	49
Cs5	0.02800	63.9−45.3	31

temperature dependence[17,21,22] with slower transformation rates at lower temperatures.

The objective of this work is to achieve selective crystallization of metastable α-form crystals with a large uniform size. The lower and upper bounds of the operating region were specified by the α-form solubility curve and metastable limit, respectively. Attenuated total reflectance-Fourier transform infrared (ATR-FTIR) spectroscopy coupled with a calibration model constructed using chemometrics techniques[24−26] was used to provide in situ solute concentration measurements. Focused beam reflectance measurement (FBRM), which measures in situ the characteristics of crystal size distribution, was used to detect the metastable limit, as previously demonstrated,[14,27,28] for the seeded system. The seeded batch cooling crystallizations were implemented with concentration feedback control at different supersaturation profiles to obtain the most appropriate batch recipe for selectively growing metastable L-glu acid crystals.

Experimental Procedures

Materials and Instruments. The instrumentation setup for the crystallization experiments is similar to that described in a previous study.[14] A Dipper-210 ATR immersion probe (Axiom Analytical) with ZnSe as the internal reflectance element attached to a Nicolet Protégé 460 FTIR spectrophotometer was used to obtain the aqueous L-glu acid spectra. A setting of 64 scans was used for each FTIR spectra. Degassed deionized water at 23.0 °C was used for the background measurement. The number of particles counted in solution by Lasentec FBRM was recorded every 20 seconds with version 6.0b12 of the FBRM Control Interface software. The solution temperature was controlled by ratioing hot and cold water to the jacket with a control valve using IMC-PID control.[29,30] Powder X-ray diffraction (PXRD) patterns of the L-glu acid crystals were collected offline, using the Bruker General Area Detector Diffraction System (GADDS, Bruker AXS, Inc.) with Cu $K_{\alpha 1}$ and Cu $K_{\alpha 2}$ (weighted sum) radiation and step size 0.02°. The characteristic peaks of both forms in the PXRD patterns (Figure 4) are consistent with a previous report.[20] L-Glu acid crystals obtained commercially (99%, Sigma Aldrich) were verified by PXRD measurements to be β-form; the characteristic peaks of the α-form were absent. α-Form crystals used for solubility measurement and as seeds in the metastable limit and batch crystallizations experiments were obtained from rapid cooling,[21,22] and the purity was similarly verified using PXRD. Scanning electron microscopy (SEM) samples were sputtered with 4−8 nm of Au/Pd before being recorded with a JEOL 7000F SEM.

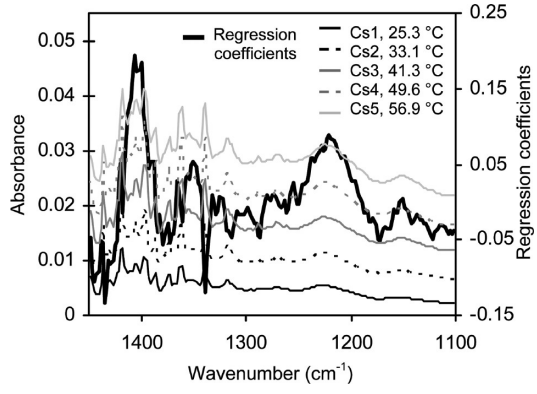

Figure 5. Representative ATR-FTIR spectra of the calibration samples and regression coefficients of the calibration model relating absorbance to solute concentration (the regression coefficients for the temperature and the intercept are not shown).

Table 2. Initial Solute Concentrations in the Metastable Limit Experiments

run	initial solute concentration, g/g of solvent
1m	0.01590
2m	0.01722; 0.01719
3m	0.01868
4m	0.02018; 0.02022
5m	0.02179

Calibration for Solution Concentration. Different solute concentrations of L-glu acid in 400 g of deionized water (Table 1) were placed in a 500-mL jacketed round-bottom flask and heated until all of the crystals dissolved. The solution was agitated with an overhead mixer with a stirring speed of 250 rpm. The solution was cooled at 0.5 °C/min, while the IR spectra were collected. The measurements were stopped once crystals started to appear. The IR spectra of aqueous L-glu acid in the range 1100−1450 cm^{-1} were used to construct the calibration model. At the given frequency range, the largest positive regression coefficient was observed at 1400−1405 cm^{-1} (Figure 5). This corresponded to the largest peak, which was due to the carboxylate stretching band in the IR spectra. The calibration model relating the IR spectra and temperature to solute concentration was determined using various chemometrics methods such as principal component regression (PCR) and partial least squares regression (PLS).[31] The calculations were carried out using in-house MATLAB 5.3 (Mathworks, Inc) code except for the PLS method, which was from the PLS Toolbox 2.0. The mean width of the prediction interval was used as the criterion to select the most accurate calibration model. The noise level of 0.001 was selected based on the compatibility of the prediction interval with the accuracy of the solubility data. The forward selection PCR 2 method[32] was selected, which gave the smallest prediction interval. The prediction interval (±0.00037 g/g of solvent) was comparable with the deviations of the experimental data points from the fitted solubility curves. The resulting calibration model had the form

$$C = \sum_{j=1100}^{1450} w_j a_j + w_T T + w_0 \qquad (1)$$

where C is the solute concentration (g/g of solvent), a_j is the absorbance at frequency j cm^{-1}, T is the temperature (°C), and w_i, w_T, and w_0 are regression coefficients.

Solubility and Metastable Limit Measurements. For each polymorph, the IR spectra of L-glu acid slurries were collected at different temperatures ranging from 25.0 to 60.0 °C. The slurry was equilibrated for 45 min to 1 h at each evaluated temperature point before recording the IR spectra. The equilibrium solute concentration

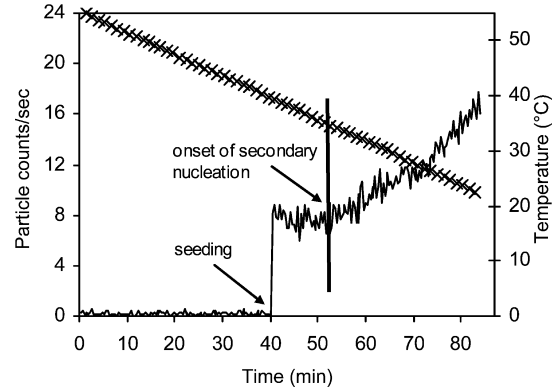

Figure 6. Particle counts/s (−) and temperature (x) profiles in the metastable limit experiment.

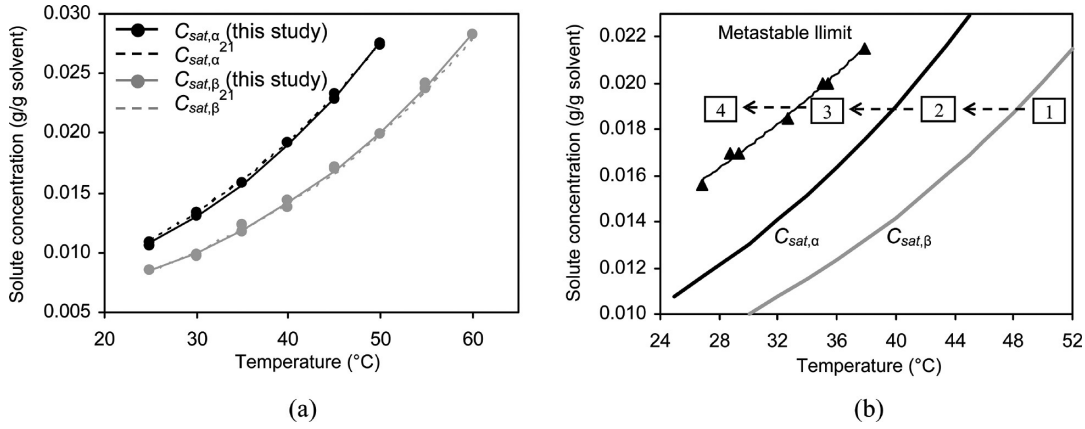

Figure 7. L-Glu acid solubility curves compared to (a) previously published data,[21] (b) metastable limit for cooling rate at 0.4 °C/min.

Table 3. Fitting Parameters for α -and *β*-Form L-Glu Acid Solubility Curves

fitting parameters	α-form	*β*-form
$b_{0,i}$	4.208×10^{-3}	3.555×10^{-3}
$b_{1,i}$	3.767×10^{-2}	3.460×10^{-2}

was then calculated using the aforementioned calibration model. The allocated time was deemed sufficient for equilibration as the recorded solute concentration profile did not show any further changes, indicative of saturation. The measurements were performed twice at the evaluated temperature points.

The metastable limit of L-glu acid solutions was determined at various solute concentrations as listed in Table 2, using the polythermal method.[33] Each solution was heated to 5.0 °C above its saturation temperature and maintained at 1 h, before cooling at 0.4 °C/min. As the main crystallization experiments utilized seeding, the metastable limit was determined for the seeded system; α-form seed crystals (0.23 g, 100−300 μm) were added at 2.0 °C after the solution temperature crossed the α-form saturation temperature. The number of the crystals in solution was monitored using FBRM. The start of a sharp increase in the particle counts/s after seeding (Figure 6) was considered to be the onset of secondary nucleation at the metastable limit, which was then plotted based on the solute concentration and temperature corresponding to the time points when the nucleation events were detected in all five experiments. No weighting of the particle counts/s profile was used. Square- and volume-weighting of the particle counts/s tended to give delayed detection of nucleation, while 1/length weighting was more susceptible to background noise. In both the solubility and metastable limit experiments, the solvent mass and the stirring speed of the overhead mixer were similar to that for calibration.

Seeded Batch Crystallization. Appropriate amounts of L-glu acid in deionized water (400 g) was heated to an initial temperature of 55.0 °C (5.0 °C above the *β*-form saturation temperature) to create an undersaturated solution with a solute concentration of 0.02000 g/g of solvent. The stirring conditions were the same as that used previously. The crystallizer was then cooled at 0.4 °C/min to 39.5 °C (2.0 °C below the α-form saturation temperature), upon which α-form seed crystals were added. The mass and size distribution of the seeds were similar to that in the metastable limit experiments. The seed mass, W_s, represented a seed loading ratio W_s/W_y of about 0.09, where W_y is the expected yield. Preset supersaturation profiles were followed during crystallization using concentration feedback control based on in situ solute concentration measurement as described previously.[14,15] The control algorithm was started shortly after seeding. Supersaturation set point profiles were selected at different constant absolute supersaturation, $\Delta C_\alpha = C - C_{sat,\alpha}$, and relative supersaturation, $\Delta C_{r,\alpha} = \Delta C_\alpha / C_{sat,\alpha}$, with respect to the α-form, where $C_{sat,\alpha}$ (g/g of solvent) is the solubility of the α-form. A preliminary run was carried out similarly at constant ΔC_α but at a higher initial solute concentration, 0.02800 g/g of solvent, with correspondingly higher operating temperature range, where initial and seeding temperature were at 65.0 and 48.3 °C, respectively.

Results and Discussion

Solubility and Metastable Limit Measurements. The solubility curves of both α- and *β*-forms of L-glu acid are in good agreement with available solubility data (Figure 7a).[21] The largest discrepancy for the α-form amounted to −0.00025 g/g of solvent (−2.3%) while that for the *β*-form was 0.00058 g/g of solvent (2.1%). The dissimilarities for the *β*-form exceeded the prediction interval of the calibration model but can be attributed to differences in the purity of the solute and solvent used. The solubility curves were fit to

$$C_{sat,i} = b_{0,i} \exp(b_{1,i} T) \quad (2)$$

where i denotes α- or *β*-forms and $C_{sat,i}$ (g/g of solvent) is the solubility (see Table 3). The maximum deviation of the experimental data points from the fitted solubility curves (−0.00033 and 0.00037 g/g of solvent for the α- and *β*-forms, respectively) were comparable with the prediction interval. The solubility measurement of the metastable form using the above method applies only if the dissolution of this form is relatively faster than its transformation to the stable form so that equilibrium with respect to the metastable form is achievable, as is the case of L-glu acid for the studied temperature range.[20]

To determine the metastable limit of the seeded system, a cooling rate of 0.4 °C/min was sufficiently fast to cool an undersaturated solution (region 1 in Figure 7b) across both solubility curves (into region 3) to achieve supersaturation with respect to the α-form, with no significant nucleation until the metastable limit was reached. This provided a window (region 3) to seed and grow α-form crystals in a controlled manner. Further cooling (into region 4) would increase the driving force to grow the seed crystals, but uncontrolled secondary nucleation would occur once the metastable limit is crossed. The metastable limit provides an estimate of the maximum allowable supersaturation for the selective and controlled growth of α-form seed crystals without any uncontrolled secondary nucleation. Using cooling rates lower than 0.4 °C/min led to primary nucleation before any seeding opportunity, either in region 2 or very close to $C_{sat,\alpha}$ in region 3. Primary nucleation in region 2 resulted in *β*-form crystals, while that in region 3 produced both forms. In either case, unintended primary nucleation is detrimental to the selective and controlled growth of the α-form seed crystals in terms of the product crystal size distribution and purity.

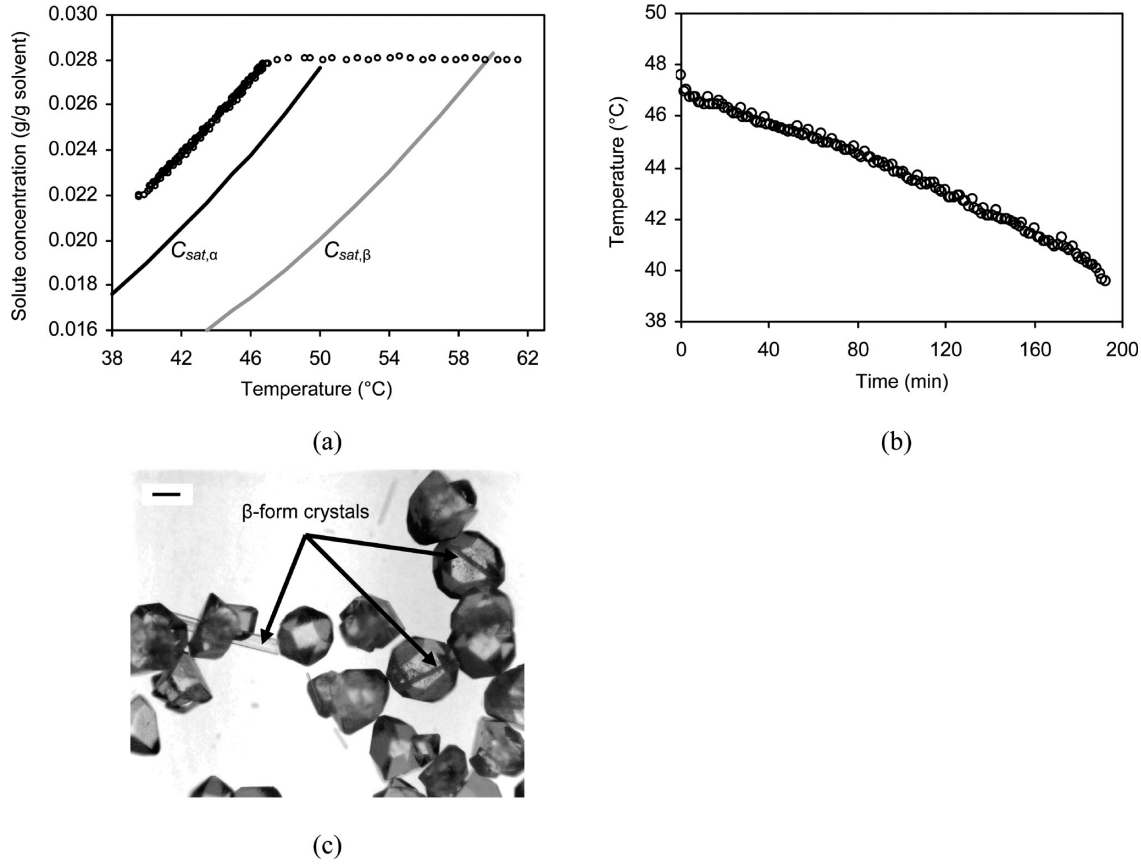

Figure 8. Preliminary seeded batch crystallization run: (a) implemented supersaturation profile, (b) temperature profile with seeding at 0 min, (c) microscopy image of the α-form product crystals with β-form crystals observed on the α-form crystal surfaces (scale bar = 180 μm).

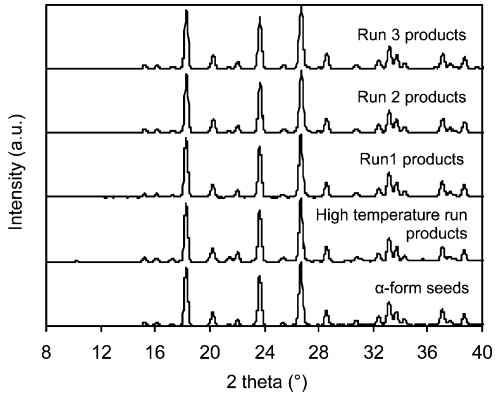

Figure 9. PXRD patterns of the seed and product crystals.

Table 4. PXRD Analysis of Seed and Product Crystals

sample	estimated solid composition[a] (wt % β-form)
seeds	0.48, 0.23; average = 0.36
high temperature run products	7.55, 7.78; average = 7.67
Run 1 products	0.00, 0.43; average = 0.22
Run 2 products	1.37, 1.08; average = 1.23
Run 3 products	0.96, 1.03; average = 0.93

[a] The polymorph composition was calculated using a convolution-based profile-fitting algorithm[37] available in the Diffracplus Topas (version 3.0, AXS Bruker Inc.) software, based on lattice parameters and atomic coordinates.[18,38] Both α- and β-forms are orthorhombic with space group $P2_12_12_1$.[18,38] The solid composition measurements have an accuracy of ~1 wt %.

Concentration-Controlled Batch Crystallization. The supersaturation profile for a preliminary seeded concentration-controlled batch crystallization carried out at higher temperatures with ΔC_α at 0.00320 g/g of solvent is shown in Figure 8a, with the temperature range upon seeding from 48.3 to 39.0 °C (Figure 8b). Although the FBRM did not show an appreciable increase in the particle counts/s, needle-shaped β-form crystals were observed on the surfaces of some α-form product crystals (Figure 8c). This is consistent with past reports on the surface nucleation of β-form L-glu acid crystals.[34−36] The cross nucleation and growth of the β-form on α-form crystal surfaces did not generate significantly more "independent" particles, such that this nucleation event was not detected by FBRM. Compositional analysis based on the PXRD pattern (Figure 9) verified the polymorphic contamination (see Table 4).

Subsequent experiments utilized a lower operating temperature range, 39.5 to 25.0 °C, to avoid cross nucleation of β-form crystals. Runs 1 and 2 were carried out with ΔC_α at 0.00420 and 0.00320 g/g of solvent, respectively, and Run 3 at $\Delta C_{r,\alpha} = 0.212$ (Figure 10a). The supersaturation profiles for Runs 2 and 3 remained in the metastable zone throughout the duration of the experiment, while that of Run 1 crossed the metastable limit initially and stayed very close to it for the remainder of the run. The impact of using different supersaturation profiles can be observed from the particle counts/s profiles (Figure 10c). In Run 1, an increase in the particle counts/s was observed due to secondary nucleation associated with the excessive supersaturation. For Run 2, the particle counts/s remained nearly constant except for an increase towards the end (~100 min onwards). The increase in the particle counts/s in the late stages of Run 2 is consistent with earlier findings that secondary nucleation tends to increase with crystal mass.[39] Maintaining constant $\Delta C_{r,\alpha}$

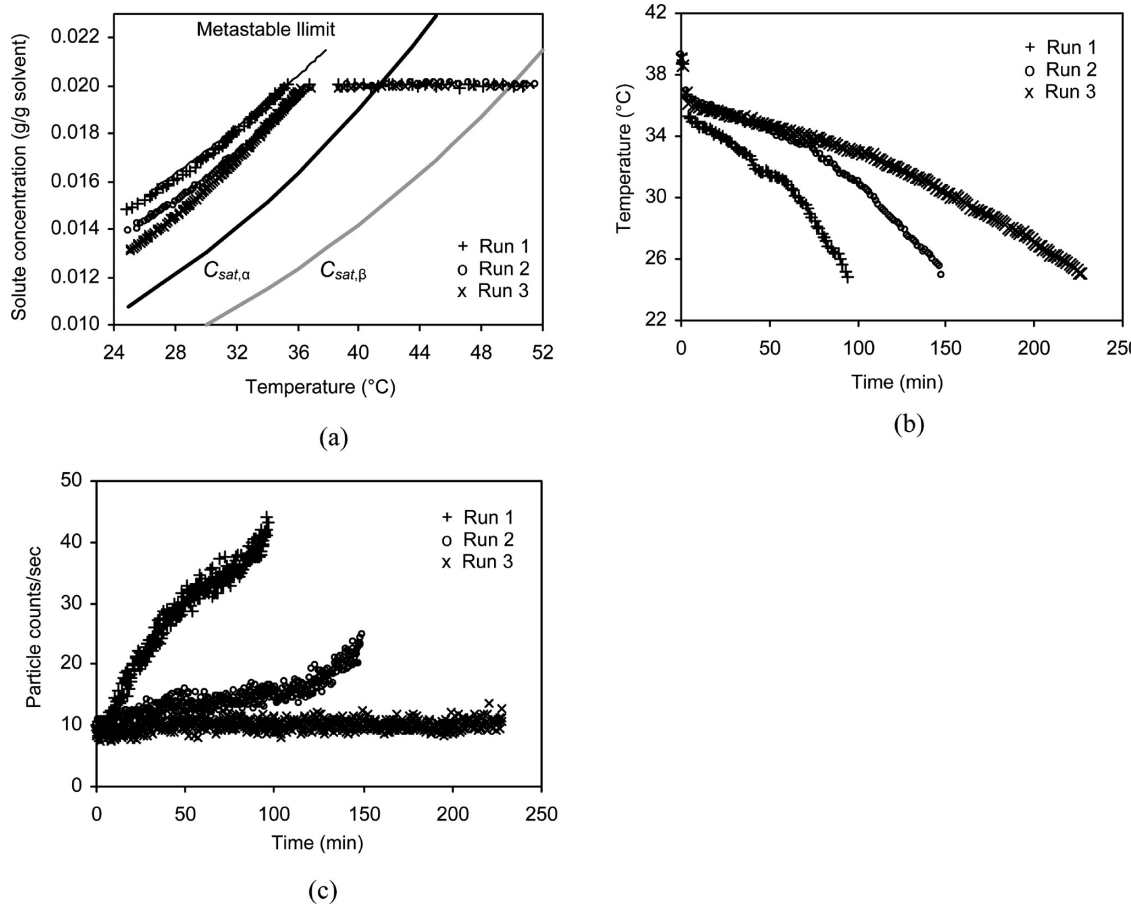

Figure 10. Seeded batch crystallization Runs 1−3: (a) implemented supersaturation profiles, (b) temperature profiles with seeding at 0 min, (c) particle counts/s profiles.

(decreasing ΔC_α) in Run 3 compensated for the effect of increasing crystal mass, to greatly suppress secondary nucleation. The recipe for Run 3 was designed following the magnitude of $\Delta C_{r,\alpha}$ in Run 2 prior to the onset of secondary nucleation (before 100 min). Solid composition analysis using PXRD patterns indicated significantly lower amounts of the β polymorph in the products of Runs 1, 2, and 3 as compared to the preliminary high temperature batch run (Table 4). For this temperature range and seeding conditions, the increase in the particle counts/s in Runs 1 and 2 was due mainly to the α-form secondary nucleation.

The change in the crystal habit of the seed from rhomboid to hexagonal (with an increase in the thickness of the crystal, see Figure 11) was consistent with past reports of α-form growth.[40] The product crystals of Runs 2 and 3 which had little or no secondary nucleation were of fairly uniform size (300−600 μm), as opposed to Run 1 (see Figure 12). Agglomeration was also observed for the Run 1 product crystals (Figure 11c). The best batch recipe implemented with concentration feedback control was that of Run 3 which gave high polymorph purity and narrow product size distribution. The polymorph purity in Run 3 as assessed by inspection of microscopy images and by PXRD was not statistically distinguishable from pure α-form crystals (Table 4).

In comparison to the rapid cooling method used to obtain the α-form seeds, homogenous nucleation is highly sensitive to local operation conditions and is often hard to reproduce.[21,22] A nucleation-based approach for selective crystallization has less reproducibility in terms of polymorph purity of the product and is less efficient particularly if there is a targeted product size range, compared to the above concentration feedback control approach based on suppression of nucleation. In the implementation of concentration-controlled crystallization in a polymorphic system, it is important to consider the cross nucleation behavior, which in this case prohibited the use of higher temperatures in the selective growth of the metastable α-form seed crystals. The temperature range utilized in Runs 1−3 was successful in maintaining high polymorph purity. β-Form secondary nucleation was averted by selecting a lower temperature range where it was known to be significantly less dominant, while α-form secondary nucleation was suppressed by avoiding excessive supersaturation. Additionally, the results from Runs 2 and 3 suggest that the metastable limit described an upper bound of the operating regime in the initial stages of crystallization, but less so towards the end due to the effect of increasing crystal mass on promoting secondary nucleation. The cooling rate used in the metastable limit experiments was similar to that in the initial stages (prior to seeding) in the concentration-controlled experiments. Upon seeding and starting concentration feedback control, the cooling rates (Figure 10b) ranged from 0.05−0.15, 0.04−0.12, and 0.03−0.07 °C/min for Runs 1, 2, and 3, respectively. As the experiment progressed, there were increasing dissimilarity in the operation conditions (specifically the mass of crystals and the cooling rate) between the metastable limit experiments and the concentration-controlled runs, and the upper bound identified in the former was no longer representative of the actual conditions

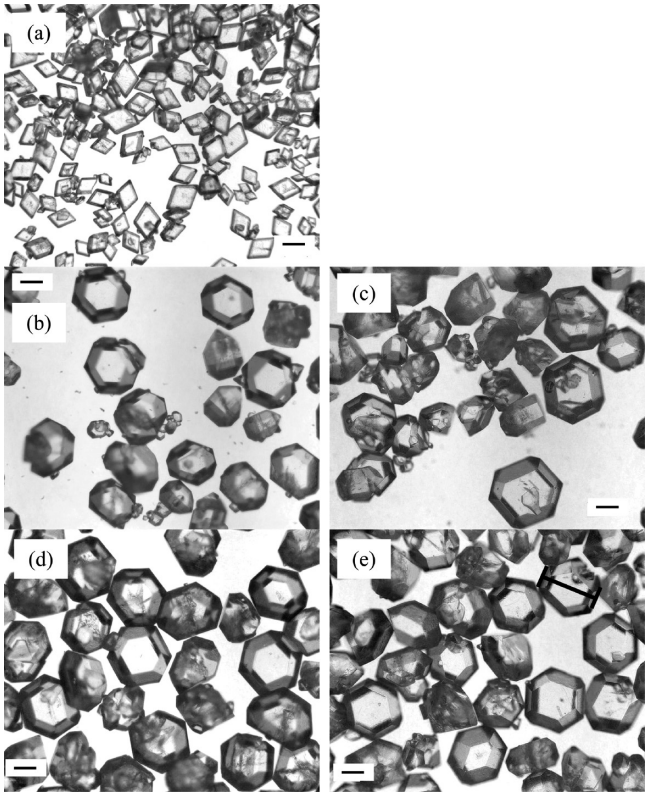

Figure 11. Microscopy images of seed and product crystals (scale bar = 180 μm): (a) α-form seed crystals, (b) α-form product crystals from Run 1 with wide size variation, (c) α-form product crystals from Run 1 with agglomeration, (d) α-form product crystals from Run 2, (e) α-form product crystals from Run 3.

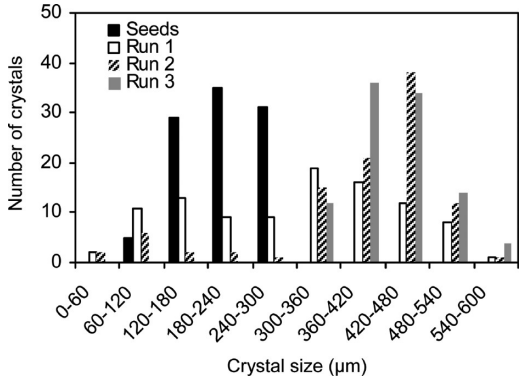

Figure 12. Size distribution of L-glu acid α-form seeds (based on the largest diagonal length) and product crystals (based on dimension indicated in Figure 11e); sample size of 100 crystals for each distribution.

in the latter. Nonetheless, appropriate batch crystallization recipes can be designed systematically based on constant relative supersaturation $\Delta C_{r,\alpha}$, using the results of earlier constant absolute supersaturation ΔC_α recipes as a more appropriate indication of the upper bound, to effectively suppress secondary nucleation in the later stages of the operation.

Conclusions

A batch recipe for the selective crystallization with uniform crystal size of the metastable form of a monotropic dimorph system, L-glutamic acid in water, was identified. The solubility curves of both α- and β-forms were determined using ATR-FTIR spectroscopy, combined with chemometrics. Laser backscattering was used to determine the seeded metastable limit. Various preset supersaturation profiles were followed during crystallization using concentration feedback control to adjust the cooling rate accordingly based on in situ solute concentration measurements. Undesired α-form secondary nucleation at the metastable limit as well as β-form secondary nucleation at high temperatures provided operating constraints in terms of the maximum allowable supersaturation and operating temperature range, respectively, for the selective crystallization of metastable α-form crystals. Batch crystallization below 40.0 °C at constant relative supersaturation suppressed both types of secondary nucleation and was successful in selectively growing large metastable crystals with uniform size. These results suggest that this may be a generic methodology for the selective growth of large crystals of the metastable form.

Acknowledgment. Mitsuko Fujiwara is acknowledged for providing technical advice on this project. The authors thank Scott Wilson from the George L. Clark X-ray facility for the PXRD data collection and analysis. The authors also thank Jim Mabon for the SEM imaging carried out in the Frederick Seitz Materials Research Laboratory Central Facilities, University of Illinois, which are partially supported by the U.S. Department of Energy under Grants DE-FG02-07ER46453 and DE-FG02-07ER46471.

References

(1) Bernstein, J. *Polymorphism in Molecular Crystals*; Clarendon Press: Oxford, 2002.
(2) Doki, N.; Yokota, M.; Kido, K.; Sasaki, S.; Kubota, N. *Cryst. Growth Des.* **2004**, *4* (1), 103–107.
(3) Doki, N.; Seki, H.; Takano, K.; Asatani, H.; Yokota, M.; Kubota, N. *Cryst. Growth Des.* **2004**, *4* (5), 949–953.
(4) Davey, R. J.; Blagden, N.; Potts, G. D.; Docherty, R. *J. Am. Chem. Soc.* **1997**, *119* (7), 1767–1772.
(5) Fujiwara, M.; Nagy, Z. K.; Chew, J. W.; Braatz, R. D. *J. Process Control* **2005**, *15*, 493–504.
(6) Nagy, Z. K.; Chew, J. W.; Fujiwara, M.; Braatz, R. D. *J. Process Control* **2008**, *18*, 399–407.
(7) Threlfall, T. *Org. Proc. Res. Dev.* **2000**, *4*, 384–390.
(8) Beckmann, W. *Org. Proc. Res. Dev.* **2000**, *4*, 372–383.
(9) Sato, K.; Boistelle, R. *J. Colloid Interface Sci.* **1983**, *94* (2), 593–596.
(10) Threlfall, T. *Org. Proc. Res. Dev.* **2003**, *7*, 1017–1027.
(11) Feng, L. L.; Berglund, K. A. *Cryst. Growth Des.* **2002**, *2*, 449–452.
(12) Liotta, V.; Sabesan, V. *Org. Process Res. Dev.* **2004**, *8*, 488–494.
(13) Gron, H.; Borissova, A.; Roberts, K. J. *Ind. Eng. Chem. Res.* **2003**, *42* (1), 198–206.
(14) Fujiwara, M.; Chow, P. S.; Ma, D. L.; Braatz, R. D. *Cryst. Growth Des.* **2002**, *2* (5), 363–370.
(15) Zhou, G. X.; Fujiwara, M.; Woo, X. Y.; Rusli, E.; Tung, H. H.; Starbuck, C.; Davidson, O.; Ge, Z.; Braatz, R. D. *Cryst. Growth Des.* **2006**, *6* (4), 892–898.
(16) Yu, Z. Q.; Chow, P. S.; Tan, R. B. H. *Ind. Eng. Chem. Res.* **2006**, *45* (1), 438–444.
(17) Kitamura, M. *J. Cryst. Growth* **1989**, *96*, 541–546.
(18) Hirayama, N.; Shirahata, K.; Ohashi, Y.; Sasada, Y. *Bull. Chem. Soc. Jpn.* **1980**, *53*, 30–35.
(19) Ni, X. W.; Valentine, A.; Liao, A.; Sermage, S. B. C.; Thomson, G. B.; Roberts, K. J. *Cryst. Growth Des.* **2004**, *4* (6), 1129–1135.
(20) Scholl, J.; Bonalumi, D.; Vicum, L.; Mazzotti, M. *Cryst. Growth Des.* **2006**, *6* (4), 881–891.
(21) Ono, T.; Kramer, H. J. M.; Horst, J. H.; Jansens, P. J. *Cryst. Growth Des.* **2004**, *4* (6), 1161–1167.
(22) Ono, T.; Horst, J. H.; Jansens, P. J. *Cryst. Growth Des.* **2004**, *4* (3), 465–469.
(23) Garti, N.; Zour, H. *J. Cryst. Growth* **1997**, *172*, 486–498.

(24) Workman, J. J.; Mobley, P. R.; Kowalski, B. R.; Bro, R. *Appl. Spec. Rev.* **1996**, *31*, 73–124.
(25) Mobley, P. R.; Kowalski, B. R.; Workman, J. J.; Bro, R. *Appl. Spec. Rev.* **1996**, *31*, 347–368.
(26) Bro, R.; Workman, J. J.; Mobley, P. R.; Kowalski, B. R. *Appl. Spec. Rev.* **1997**, *32*, 237–261.
(27) Tahti, T.; Louhi-Kultanen, M.; Palosaari, S. In *14th International Symposium on Industrial Crystallization*; Institution of Chemical Engineers: Rugby, UK, 1999; pp 1−9.
(28) Barrett, P.; Glennon, B. *Trans. Inst. Chem. Eng.* **2002**, *80*, 799–805.
(29) Braatz, R. D. In *The Control Handbook*; Levine, W. S., Ed.; CRC Press: Boca Raton, Florida, 1995; pp 215−224.
(30) Morari, M.; Zafiriou, E. *Robust Process Control*; Prentice Hall: Englewood Cliffs, New Jersey, 1989.
(31) Togkalidou, T.; Fujiwara, M; Patel, S.; Braatz, R. D. *J. Cryst. Growth* **2001**, *231*, 534–543.
(32) Xie, Y.; Kalivas, J. *Anal. Chim.* **1997**, *348*, 19–27.
(33) Nyvlt, J.; Sohnel. O.; Matuchova, M.; Broul, M. *The Kinetics of Industrial Crystallization*; Elsevier: New York, 1985.
(34) Cashell, C.; Sutton, D.; Corcoran, D.; Hodnett, B. K. *Cryst. Growth Des.* **2003**, *3* (6), 869–872.
(35) Cashell, C.; Corcoran, D.; Hodnett, B. K. *R. Soc. Chem.* **2003**, 374–375.
(36) Ferrari, E. S.; Davey, R. J. *Cryst. Growth Des.* **2004**, *4* (5), 1061–1068.
(37) *Diffracplus Topas (version 3.0) User's Manual*, April 2005; AXS Bruker Inc.: Madison, WI.
(38) Lehmann, M. S.; Koetzle, T. F.; Hamilton, W. C. *J. Cryst. Mol. Struct.* **1972**, *2*, 225–233.
(39) Randolph, A.; Larson, M. A. *Theory of Particulate Processes*; Academic Press: San Diego, CA, 1988.
(40) Kitamura, M.; Ishizu, T. *J. Cryst. Growth* **2000**, *209*, 138–145.

CG800546U